CHAPTER VI

PREPARATION OF HIGHLY ORDERED FE-SBA-1 AND TI-SBA-1 CUBIC MESOPOROUS SILICA VIA SOL-GEL PROCESSING OF SILATRANE

6.1 Abstract

Silatrane prepared from fumed silica and triethanolamine (TEA) was used as a precursor for the sol-gel synthesis of M-SBA-1 (M = Fe and Ti) at room temperature using hexadodecyltrimethylammonium bromide as a template, and dilute solutions of ferric chloride and titanium glycolate as metal sources. Powder X-ray diffraction (XRD) showed the mesoporous materials to be well-ordered cubic structures, while N_2 adsorption/desorption measurements yielded high surface areas. Diffuse reflectance UV–visible spectroscopy demonstrated that iron (Fe^{3+}) and titanium (Ti^{4+}) were incorporated crystallographically into the framework of the calcined materials to loadings of 6wt% Fe and 10wt% Ti without perturbing the ordered mesoporous structure.

6.2 Introduction

In mesoporous materials of the SBA family, phases with a three-dimensional pore system are advantageous for catalytic applications, compared to one-dimensional pore arrays, because of the thicker walls, greater pore diameters and improved hydrothermal stability with respect to reference materials such as MCM-41 [1-6]. Moreover, metal substituted mesoporous architectures are attractive for catalytic reactions involving molecules that are sterically excluded from the channels of microporous zeolites [7-9]. Recently, several metal ions including Ti^{4+}, Cr^{6+}, Mo^{5+}, V^{5+} and Fe^{3+} have been successfully incorporated into the frameworks of mesoporous silicas [10-16]. In particular, Ti-substituted molecular sieves (Ti^{4+}), such as TS-1, Ti-beta and Ti-MCM-41 have displayed excellent catalytic properties in selective oxidation reactions when using aqueous hydrogen peroxide as the oxidant

[17-20]. Iron-containing mesoporous materials (Fe^{3+}), such as Fe-SBA-1, Fe-MCM-41, and Fe-HMS have also been extensively studied because of their unique catalytic enhancement of hydrocarbon oxidation, selective reduction, acylation and alkylation reactions [3-6].

In an earlier report, the successful synthesis of SBA-1 mesoporous silica via a sol-gel process using silatrane was described [21]. Here, this approach is extended to the preparation of highly ordered M-SBA-1 (M = Fe and Ti) cubic mesoporous silicas, and the structural and physical properties of these materials evaluated.

6.3 Experimental

6.3.1 Materials

Fumed silica (SiO_2, 99.8%) (Sigma-Aldrich), titanium dioxide (TiO_2) (Carlo Erba), triethanolamine (TEA) (Carlo Erba), tetraethylenetriamine (TETA) (FACAI, Thailand), ethylene glycol (J.T. Baker, USA), acetronitrile (Labscan, Asia), ferric chloride ($FeCl_3$) (Sigma-Aldrich), hexadodecyltrimethylammonium bromide (C_{16}TMAB) (Sigma-Aldrich), H_2SO_4 (Labscan, Asia) and NaOH (Labscan, Asia) were used without treatment.

6.3.2 Preparation of silatrane and titanium glycolate precursor

The silatrane precursor was synthesized from a mixture of silicon dioxide (0.1 mol, 6 g) and triethanolamine (0.125 mol, 18.6 g) in 100 mL of ethylene glycol via the Oxide One Pot Synthesis process [22,23]. The reaction takes place at the boiling point of ethylene glycol (200°C) under a nitrogen atmosphere for 10 h, and the excess ethylene glycol removed under vacuum at 110°C to obtain the crude brown solid. Washing with acetonitrile three times gave a white powder having a theoretical ceramic yield of ~19% $N(CH_2CH_2O)_3SiOCH_2CH_2N(CH_2CH_2OH)_2$.

The titanium glycolate precursor [24] was prepared by combining titanium dioxide (0.1 mol, 8 g) and triethylenetetramine (0.028 mol, 14.8 g) in ethylene glycol (100 mL) that was boiled under nitrogen (200°C / 24 h). Unreacted titania was

centrifugally separated from the solution, while excess solvent and TETA were removed by vacuum distillation to obtain a white solid. This product was washed with acetonitrile three times then dried in a vacuum desiccator to obtain $Ti(OCH_2CH_2O)_2$ (yield 47%).

6.3.3 Preparation of mesoporous M-SBA-1

In this synthesis, solution A was prepared by adding C_{16}TMAB (0.44g) to water (30 ml) and stirring for 0.5 h to obtain a clear solution. Solution B was prepared by dissolving silatrane (5 mmol, 1.4g) in 14 ml of 0.3 M H_2SO_4 and NaOH (1.7 mmol, 0.068g) by stirring for 0.5 h. The required amount of metal precursor was added to solution B and stirring continued for 0.5 h. Solution B was then added to the solution A under vigorous stirring that continued for 4 h. Water (30 ml) was added to this mixture before aging for 2 days at room temperature to form a white precipitate. The product was filtered, washed with distilled water, and dried at room temperature overnight. The template was removed by calcination (560°C / 6 h) in a Carbolite Furnace (CFS 1200) at a heating rate of 0.5°C/min.

6.3.4 Characterization

The mesoporous products were characterized using a Rigaku X-ray diffractometer (XRD) with patterns accumulated at a scan speed of 1 degree/sec using CuKα radiation over the range of 2θ = 1.5-8°. MSBA-1 morphology was observed by secondary electron imaging (SEI) with a JEOL 5200-2AE scanning electron microscope (SEM), while mesopore order was directly examined using a JEOL 2010F transmission electron microscope (TEM). Specific surface area and average pore size were determined by the Brunauer-Emmett-Teller (BET) method with a Quantasorb JR instrument. Diffuse reflectance UV-visible spectroscopic measurements were recorded on a Shimadzu UV-2550 spectrometer fitted with an ISR-2200 integrating sphere attachment from 200 – 600 nm referenced to $BaSO_4$. Electron spin resonance (ESR) spectra were measured at the X-band, ~9 GHz, on a JEOL JES-RE2X spectrometer.

6.4 Results and Discussion

Higher metal (Ti^{4+}, Fe^{3+}) incorporation in SBA-1 has been attributed to a surfactant silica assembly mechanism, in which the mesophase forms under acidic conditions via an $S^+X^-I^+$ pathway (S, X and I correspond to surfactant, halide and inorganic species, respectively). As silatrane is a water soluble alkoxide, hydrolysis to silicate generates TEA molecules that act as a co-template in mesoporous formation, and in addition, reduce the net positive charge on silica [21] to enhance the interaction with metal ions and promote higher metal incorporation in SBA -1.

Diffuse reflectance UV-visible spectroscopy was used to characterize the nature and coordination of Fe^{3+} [3-6] and Ti^{4+} ions [15-18] in the SBA-1 mesoporous molecular sieves. Figure 6.1 (A and B) shows UV-visible spectra of the calcined Fe-SBA-1 and Ti-SBA-1 as a function of metal loading. For Fe-SBA-1, all samples showed a strong UV band at ~230 nm associated with a shoulder at 290 nm consistent with Laporte-allowed ligand-to-metal charge transfer involving isolated $Fe^{3+}O_4$ co-ordination [5]. The intensity of these bands increases monotonically with Fe content, as expected if there is crystallographic incorporation of Fe in SBA-1. A characteristic band above 320 nm typical of octahedral co-ordination ($Fe^{3+}O_6$) was absent indicating these materials are free of ferric oxide species similar to those found in iron hydroxide, iron oxyhydroxide and iron oxide [26-28]. The Ti-SBA-1 samples show an absorption band centered at 220 nm characteristic of the charge-transfer transition associated with regular $Ti^{4+}O_4$ framework tetrahedra. Octahedral co-ordination ($Ti^{4+}O_6$) is unlikely as the distinctive feature at 330 nm is missing [15-18].

The X-band ESR spectra of the calcined Fe-SBA-1 (Fig. 6.2) shows two major components at g = 4.3, assigned to high-spin Fe^{3+} in a distorted tetrahedral environment, and g = 2.0, attributed to high-spin Fe^{3+} in a symmetrical tetrahedral/octahedral coordination [3-6]. With increasing iron content, the corresponding ESR signals increase in intensity. The observation of the g = 2.0 signal alone cannot be taken as unambiguous evidence for iron framework substitution unless combined with other physical or chemical methods, because of possible contributions from extra-framework Fe^{3+} [28-30].

Small angle XRD confirmed that after calcination, ordered mesopores were obtained regardless of the metal (Fe/Ti) loading (Fig. 6.3). SBA-1 displays three well resolved diffraction peaks in the region of 2θ = 1.5-3° which can be indexed as (200), (210) and (211) reflections with respect to a cubic lattice [25-27], that persists to an iron loading of 6 wt% (Fig. 6.3A). A similar trend was observed to the Ti-loaded samples (Fig. 6.3B) although the reflections are somewhat broader. Dilation of the d_{210} spacing of Ti-SBA-1 with increasing titanium loading confirms the substitution of titanium (Ti^{4+} = 0.42 Å) for silicon (Si^{4+} = 0.26 Å) in the framework [17-20].

Since the radius of the ionic Fe^{3+} is larger than that of Si^{4+} (r^{3+}_{Fe} = 0.49 Å and r^{4+}_{Si} = 0.26 Å), dilation of a_0 (Table 6.1) is consistent with Fe^{3+} incorporation in the SBA-1 framework [26]. However, the decrease in intensity of the (200) and (211) reflections, with an increasing iron content, suggests a reduction in the degree of ferrosilicate polymerization and structural order [26]. Generally, it is expected that the unit cell parameter will be enlarged after the incorporation of metal cations with ionic radii larger than Si^{4+}.

Transmission electron microscope lattice images (Fig. 6.4A and B) of representative Ti-SBA-1 and Fe-SBA-1 crystals demonstrates that regular mesopore arrays had formed, and exclude the presence of metal segregation, as this would be readily detected due to the greater electron scattering powder of Fe/Ti compared to Si.

The N_2 adsorption/desorption isotherms of calcined Fe- and Ti-SBA-1 were all type IV (Fig. 6.5) and showed steep increases in the volume of adsorbed nitrogen at relative pressures of P/P_0 = 0.1-0.3 due to the onset of capillary condensation within uniform mesopores. Both Fe- and Ti-SBA-1 possessed a narrow pore size distribution with an average pore diameter of ~2 nm confirming the TEM observations. The incorporation of higher metal contents decreases the specific surface area from 1435 to 880 m^2/g.

6.5 Conclusions

Silatrane obtained from the Oxide One Pot Synthesis (OOPS) process is a highly reactive precursor for the preparation of transition metal-bearing SBA-1 mesoporous materials. It has been demonstrated that the SBA-1 framework can accommodate up to 6wt% Fe and 10wt% Ti without perturbing mesopore order. Dilation of the mesoporous lattice with metal loading is consistent with crystallochemical framework replacement of Si^{4+} by Fe^{3+} / Ti^{4+} and the predominant retention of the metals in tetrahedral co-ordination to oxygen. However, to maintain charge balance as Fe^{3+} replaces Si^{4+} some edge-sharing octahedral FeO_6 clusters may be present as suggested by ESR spectroscopy.

6.6 Acknowledgements

This research work is financially supported by the Postgraduate Education and Research Program in Petroleum and Petrochemical Technology (ADB) Fund, the Ratchadapisake Sompote Fund, Chulalongkorn University and the Thailand Research Fund (TRF).

6.7 References

1. S. Bordiga, R. Buzzoni, F. Geobaldo, C. Lamberti, E. Giamello, A. Zecchina, G. Leofanti, G. Petrini, G. Tozzola, G. Vlaic, *J. Catal.*, 158, 486-501 (1996).
2. G. Grubert, M. Hudson, R. Joyner, M. Stockenhuber, *J. Catal.*, 196, 126-33 (2000).
3. A. Vinue, T. Krithiga, V. Murugesan, W. Bohlmann, V. Umamaheswari, A. Poppl, M. Hartmann, *Appl. Catal. A: Gen.*, 265, 1-10 (2004).
4. A. Vinue, T. Krithiga, V. Murugesan, M. Hartmann, *Adv. Mater.*, 16, 1817-21 (2004).
5. A. Vinue, T. Krithiga, V.V. Balasubramanian, A. Asthana, P. Srinivasu, T. Mori, K. Agira, G. Ramanath, P.G. Ganesan, *J. Phys. Chem. B*, 110, 11924-31 (2006).

6. A. Vinu, T. Krithiga, N. Gokulakrishnan, P. Srinivasu, S. Anandan, K. Agira, V. Murugesan, V.V. Balasubramanian, T. Mori, *Micropor. Mesopor. Mater.*, 100, 87-94 (2007).
7. M. Selvaraj, A. Pandurangan, K.S. Seshadri, P.K. Sinha, V. Krishnasamy, K.B. Lal, *J. Mol. Catal. A: Chem.*, 186, 173-86 (2002).
8. S.K. Jana, H. Takahashi, M. Nakamura, M. Kaneko, R. Nishida, H. Shimizu, T. Kugita, S. Namba, *Appl. Catal. A: General.*, 245, 33-41 (2003).
9. Q. Huo, D.I. Margolese, D.I. Ciesla, D.G. Demuth, P. Feng, T.E. Gier, P. Sieger, A. Firouzi, B.F. Chemelka, F. Schu¨ th, G.D. Stucky, *Chem Mater.*, 6, 1176-91 (1994).
10. Q. Huo, D.I. Margolese, U. Ciesla, D.G. Demuth, P. Feng, T.E. Gier, P. Sieger, A. Firouzi, B.F. Chemelka, G.D. Stucky, *Chem. Mater.*, 8, 1147-60 (1996).
11. A. Vinu, J. Dedecek, V. Murugesan, M. Hartmann, *Chem. Mater.*, 14, 2433-5 (2002).
12. X. Zhao, X. Wang, *J. Mol. Catal. A: Chem.*, 261, 225-31 (2007).
13. L.X. Dai, Y.H. Teng, K. Tabata, E. Suzuki, T. Tatsumi, *Micropor. Mesopor. Mater.*, 44-45, 573-80 (2001).
14. L.X. Dai, K. Tabata, E. Suzuki, T. Tatsumi, *Chem. Mater.*, 13, 208-12 (2001).
15. D. Ji, T. Ren, L. Yan, J. Suo, *Mater. Lett.*, 57, 4474-7 (2003).
16. D. Ji, R. Zhao, G. Lv, G. Qian, L. Yan, J. Suo, *Appl. Catal. A: General.*, 281, 39-45 (2005).
17. R.H.P.R. Poladi, C.C. Landry, *Micropor. Mesopor. Mater.*, 52, 11-8 (2002).
18. V.N. Rajakovic, S. Mintova, J. Senker, T. Bein, *Mater. Sci. Eng. C*, 23, 817-21 (2003).
19. R. Anand, M.S. Hamdy, P. Gkourgkoulas, Th. Maschmeyer, J.C. Jansen, U. Hanefeld, *Catal. Today*, 117, 279-83 (2006).
20. N. Thanabodeekij,W. Tanglumlert, E. Gulari, and S.Wongkasemjit, *Appl. Organomet. Chem.*, 19, 1047–54 (2005).
21. W. Tanglumlert, T. Imae, T. J. White, S. Wongkasemjit, *J Am Ceram.Soc.*, 90, 3992-7 (2007).

22. V. Jitchum, C. Sun, S. Wongkasemjit, H. Ishida, *Tetrahedron*, 57, 3997-4003 (2001).

23. W. Charoenpinijkarn, M. Suwankruhasn, B. Kesapabutr, S. Wongkasemjit, A.M. Jamieson, *J. Eur. Polym.*, 37, 1441-8 (2001).

24. N. Phonthammachai, T. Chairassameewong, E. Gulari, A.M. Jamieson, S. Wongkasemjit, *J. Met. Mat. Min.* 12, 23-8 (2002).

25. M. W. Anderson, C. C. Egger, G. J. T. Tiddy, J. L. Casci, and K. A. Brakke, *Angew. Chem. Int.*, 44, 3243–8 (2005).

26. A. Tuel, S. Gontier, *Chem. Mater.*, 8, 114-22 (1996).

27. Y. Li, Z. Feng, Y. Lian, K. Sun, L. Zhang, G. Jia, Q. Yang, C. Li, *Micropor. Mesopor. Mater.*, 84, 41-9 (2005).

28. D. Goldfarb, M. Bernardo, K.G. Strohmaier, D.E.W. Vaughan, H. Thomann, *J. Am. Chem. Soc.*, 116, 6344-53 (1994).

29. P. Selvam, S.K. Mohapatra, *J. Catal.*, 238, 88-99 (2006).

30. K. Bachari, J.M.M. Millet, P. Bonville, O. Cherifi, F. Figueras, *J. Catal.*, 249, 52-8 (2007).

Table 6.1 Physical and crystallographic characteristics of M-SBA-1 ($M = Fe^{3+}$, Ti^{4+}) mesoporous materials as a function of metal loading

Material		Physical Properties			Crystallographic Properites	
Designation	Metal Doping (wt %)	BET Surface Area (m^2/g)	Pore Volume (cm^3/g)	Average Pore Diameter (nm)	d_{210} (nm)	a_0 (nm)
SBA-1	0	1435	0.75	2.12	3.62	8.09
Fe 2%	2	1164	0.61	2.11	3.65	8.16
Fe 4%	4	1175	0.61	2.11	3.68	8.23
Fe 6%	6	1062	0.54	2.10	3.71	8.30
Ti 2%	2	1101	0.57	2.07	3.77	8.43
Ti 4%	4	1029	0.56	2.17	3.80	8.51
Ti 6%	6	880	0.51	2.34	3.83	8.58

[a] Lattice parameters a_0 were calculated based on the formula $a_0 = \sqrt{5}d_{210}$

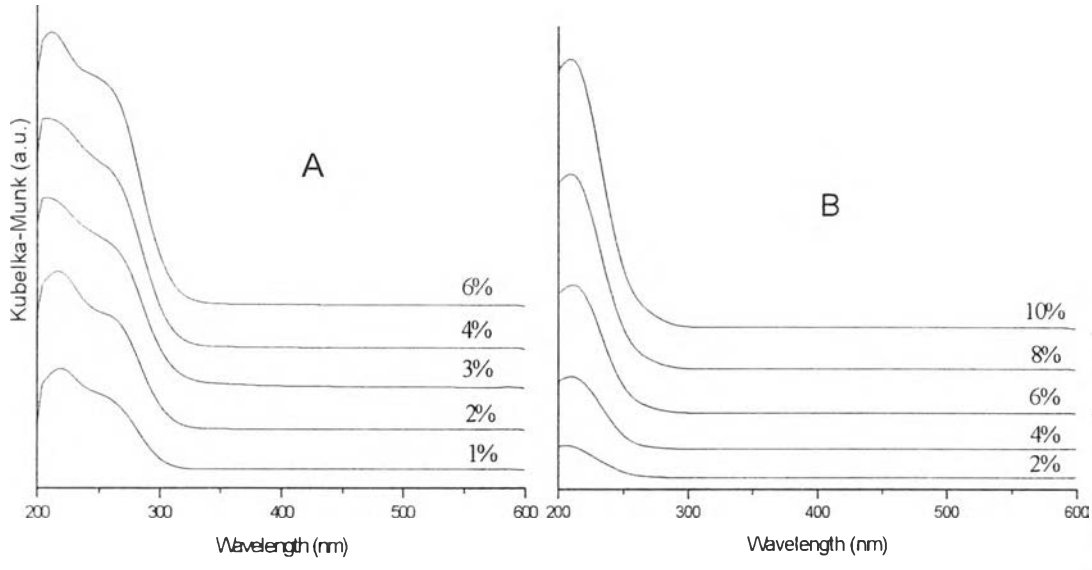

Figure 6.1 Diffuse reflectance UV-visible spectra of calcined Fe-SBA-1 (A) and Ti SBA-1 (B) mesoporous materials as a function of crystallochemically incorporated metal loading.

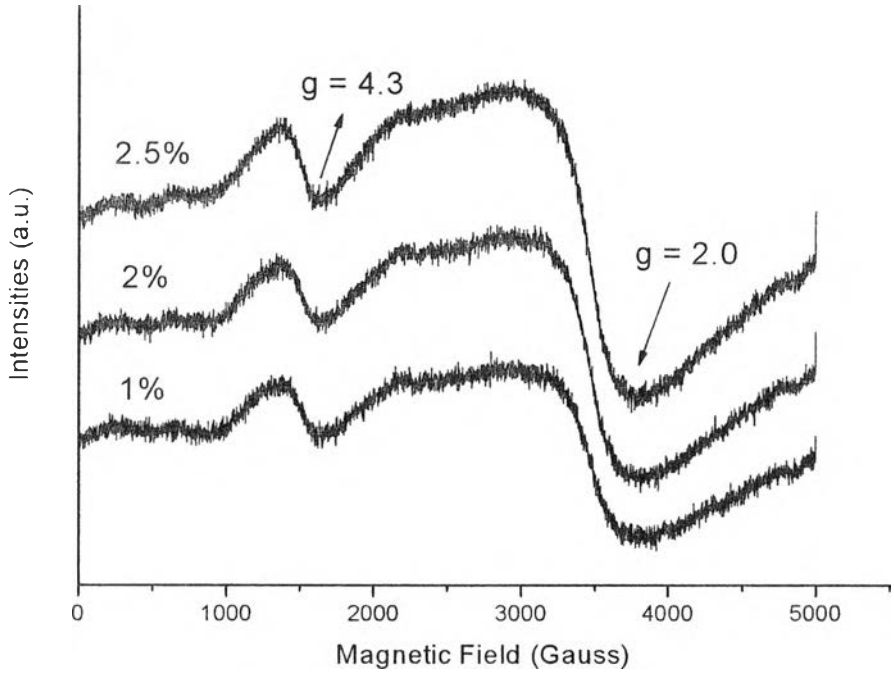

Figure 6.2 ESR spectra of calcined Fe-SBA-1 materials of different iron content.

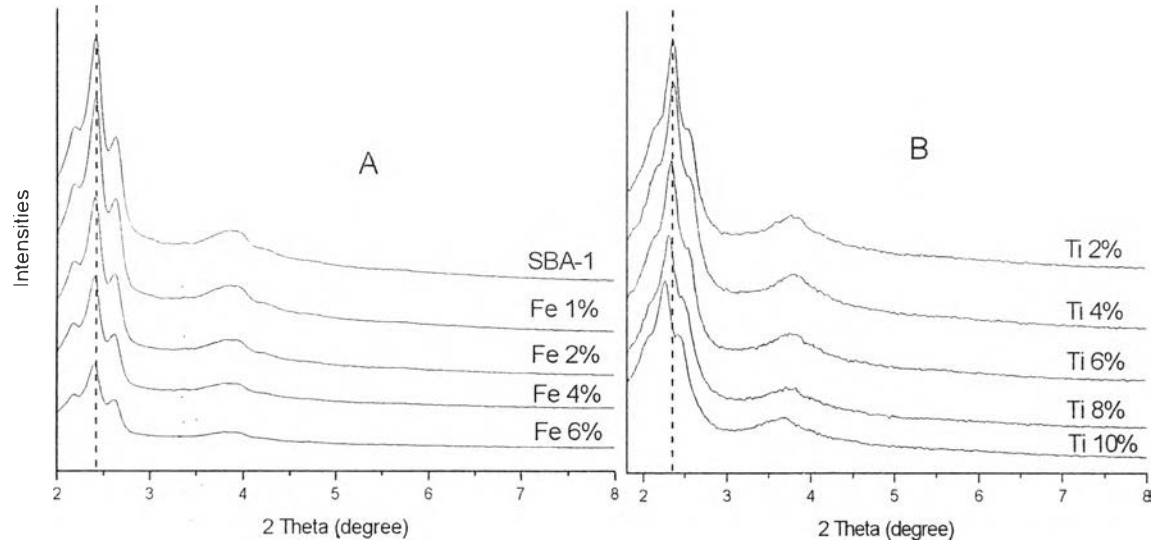

Figure 6.3 XRD patterns of calcined Fe-SBA-1 (A) and Ti-SBA-1 (B) containing different metal loadings.

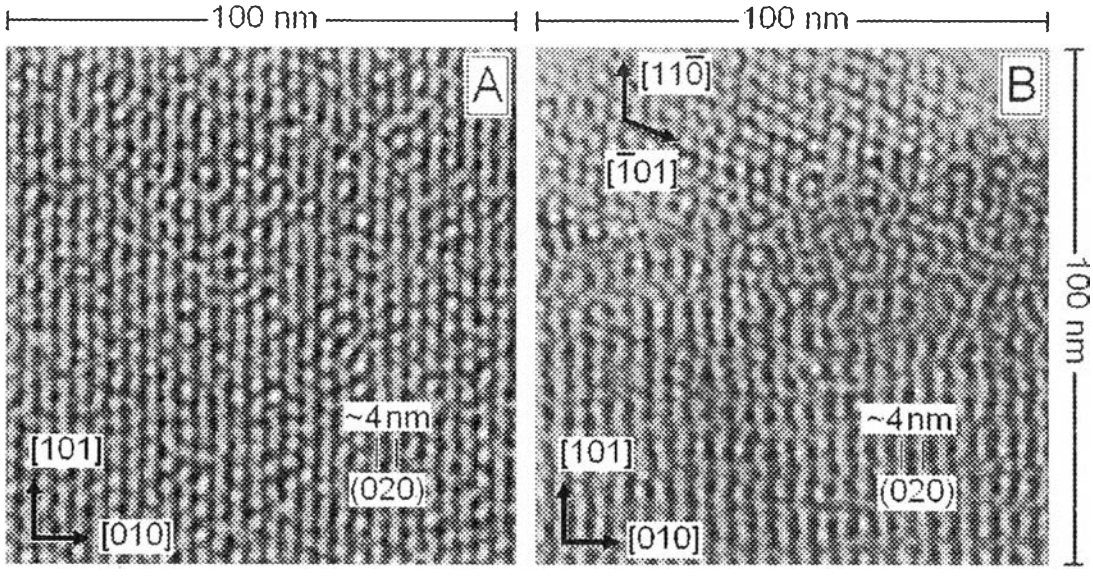

Figure 6.4 Typical bright field TEM images of calcined M-SBA-1 at Fe 4% (A) and Ti 4% (B) metal loadings. The imaging conditions are selected so that white dots indicate mesopore columns, with the micrographs labeled according to a cubic cell, and orientated in [-101]. Ordering is well developed along [010], but less so in [101], and for all materials, commonly extended for several nanometres. In the upper part of (B) a [111] crystal fragment extends under the [-101] fragment to create a Moiré interference pattern, confirming the mesopore order of each part.

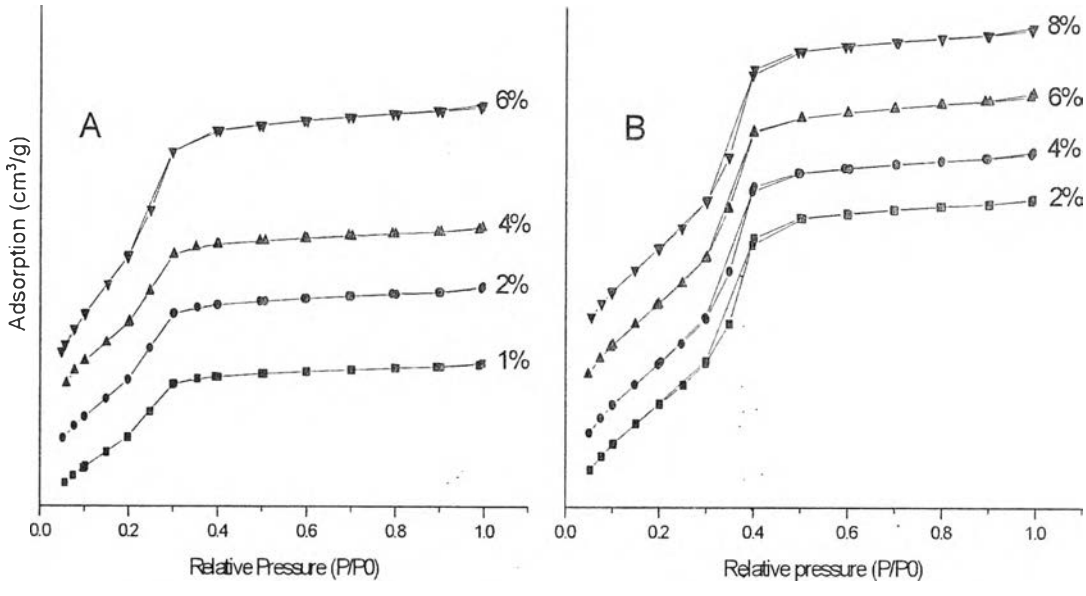

Figure 6.5 Nitrogen adsorption–desorption isotherms of calcined Fe-SBA-1 (A) and Ti-SBA-1 (B) with different metal loadings.